Emergence of high-connectivity states before epileptic seizures: Multi-patient validation, physiological correlates, and network modeling

Nicolas Medina*[1], Manel Vila-Vidal[1,2], Ana Tost[1], Mariam Khawaja[3], Mar Carreño[3,4], Pedro Roldán[5], Jordi Rumià[5], María Centeno[3,4], Estefanía Conde[3,4], Antonio Donaire[3,4,6], Adrià Tauste Campo*[1]

[1] Computational Biology and Complex Systems Group, Department of Physics, Universitat Politècnica de Catalunya, Barcelona, Spain

[2] BrainFocus Labs, SL, Barcelona, Spain

[3] Epilepsy Program, Hospital Clínic, Barcelona, Spain

[4] Institut d'Investigacions Biomèdiques August Pi i Sunyer (IDIBAPS), Barcelona, Spain

[5] Epilepsy Program, Neurosurgery, Hospital Clínic, Barcelona, Spain

[6] CIBERBBN, Networking Centre on Bioengineering, Biomaterials and Nanomedicine, Barcelona, Spain

∗Corresponding authors: Address: Computational Biology and Complex Systems, Department of Physics, Universitat Politècnica de Catalunya, 08028, Barcelona, Spain. E-mail: brian.nicolas.medina@upc.edu, adria.tauste@upc.edu.

Abstract

Epilepsy affects approximately 50 million people worldwide, making it one of the most prevalent neurological disorders. Predicting seizures through reliable pre-seizure biomarkers could greatly enhance neuromodulation therapies for drug-resistant patients. Recent research using stereo-electroencephalography (sEEG) has revealed specific changes in network dynamics during pre-seizure periods. In particular, our previous work demonstrated that day-time dependent alterations preceding seizures are largely driven by an increased occurrence of recurrent, short-lasting (0.6s) high-connectivity network configurations, termed High-Connectivity States (HCS). In this study, we replicated these findings using long-term sEEG recordings from a publicly available database and another patient undergoing presurgical evaluation with depth electrodes. For the latter patient, we leveraged all available monitoring information to validate the robustness of HCS alterations across different recording configurations. Additionally, we compared HCS dynamics with other sEEG measurements (e.g., power activity) and electrocardiogram-derived variables (e.g., heart rate) and developed a low-dimensional statistical network model to capture key network features of the pre-seizure period. Our results confirmed the specific emergence of HCS hours before seizure onset, consistent across monopolar, bipolar, and common average referential recordings. Notably, preictal HCS probability alterations were distributed across the frequency power spectrum and exhibited stronger correlations with heart rate fluctuations than with grand-average functional connectivity. The statistical model indicated that preictal HCS probability changes arise from shifts in network topology rather than changes in mean connectivity, highlighting the role of complex interactions between epileptogenic and non-epileptogenic brain regions. These findings suggest that integrating HCS probability with both invasive and non-invasive monitoring variables could establish it as a promising biomarker for an early detection of upcoming epileptic seizures.

Keywords: epilepsy, stereoelectroencephalography, functional connectivity, network states, heart rate, seizure-onset zone, statistical network model.

1. INTRODUCTION

Epilepsy is the fourth most common neurological disorder worldwide, affecting approximately 0.5–1% of the global population (Sander, 2013). This disorder is characterized by recurrent seizures, resulting from abnormal and excessive electrical activity in the brain (Sazgar & Young, 2019). Despite significant advances in treatment, 30–40% of patients develop drug-resistant epilepsy (Sharma et al., 2015), which poses substantial clinical challenges. For these patients, surgical intervention remains the most effective strategy to control seizures and improve quality of life. Accurate pre-surgical diagnosis, often based on continuous intracranial monitoring using stereo-electroencephalography (sEEG), is instrumental in localizing the seizure onset zone (SOZ) and mapping seizure propagation networks.

The identification of pre-seizure periods in real time remains a key challenge with critical implications for the development of adaptive neuromodulation therapies. Such therapies, which aim to modulate brain activity in response to detected pre-seizure states, hold great promise for improving outcomes in drug-resistant patients (Park et al., 2020). To enable these approaches, it is essential to characterize the changes in brain network dynamics that occur during the pre-seizure phase. In this context, recent studies have resorted to functional connectivity measures, such as coherence and phase-locking values, combined with graph-theoretical metrics (e.g., clustering coefficient and node centrality), to identify neural network features preceding seizures (Lehnertz et al., 2023). In addition, independent research has shown that the functional connectivity of hippocampal networks fluctuates over multiday cycles, aligning with seizure likelihood patterns (Haneef et al., 2014). More recently, it has been shown that connectivity-based biomarkers derived from brief recordings can predict seizure likelihood with accuracy comparable to complex models (Khambhati et al., 2024). On the other hand, studies examining resting-state sEEG connectivity patterns have further identified key biomarkers that might serve as reliable indicators of seizure risk (Cousyn et al., 2023). Along this line of work, (Tauste Campo et al., 2018) demonstrated that network dynamics become less variable preceding seizures, a phenomenon primarily explained by changes in the probability of short-lasting (0.6s) high-connectivity states (HCS). This reduced variability reflects altered brain network dynamics in the pre-ictal phase and highlights the potential of HCS dynamics as predictive biomarkers extending beyond the SOZ to involve distributed brain regions.

Nowadays, trends in seizure forecasting highlight the importance of integrating

physiological variables from diverse sources, including electrocardiogram (ECG) signals and circadian rhythms (Vandecasteele et al., 2021). Notably, autonomic dysregulation, including seizure-induced tachycardia or bradycardia, has been observed in patients with temporal lobe epilepsy and could serve as a complementary pre-seizure biomarker (Billeci et al., 2018). Combining neural network dynamics with physiological markers offers a more holistic approach to seizure prediction, potentially enabling precise therapeutic interventions (R. S. Fisher et al., 2014).

In the present study, we expand on the findings of (Tauste Campo et al., 2018) by investigating HCS dynamics as a potential biomarker for pre-seizure identification. In a cohort of eleven patients undergoing intracranial sEEG monitoring, we demonstrate that reduced variability in network dynamics preceding seizures is primarily driven by altered HCS probabilities. In one patient with complete data, we further validated the robustness of HCS probabilities across different referencing montages and explored correlations between HCS probabilities, sEEG power, heart rate fluctuations, and connectivity-based measures. Finally, we developed a statistical model to reproduce the emergence of HCS, providing a framework for future studies aimed at understanding the changes at a functional network level that precede epileptic seizures.

2. METHODS

Patients and recordings

This study utilized stereoelectroencephalography (sEEG) recordings obtained prior to the first recorded spontaneous clinical seizure in one patient with pharmacoresistant focal-onset epilepsy. The patient underwent presurgical evaluation at the Epilepsy Unit of Hospital Clínic in Barcelona, Spain, and the clinical characteristics are summarized in Table 1. sEEG recordings were performed using a standard clinical intracranial EEG system (XLTEK, Natus Medical) with a sampling rate of 2048 Hz. Intracranial multichannel electrodes (Dixi Medical, Besançon, France; diameter: 0.8 mm; 5–18 contacts, contact length: 2 mm, inter-contact distance: 1.5 mm) were stereotactically implanted using frameless stereotaxy, neuronavigation assistance, and intraoperative CT-guided O-Arm imaging with the Vertek articulated passive arm. Electrode implantation decisions, target selection, and monitoring durations were determined based on clinical requirements. This patient provided informed consent for the use of their sEEG data in research. sEEG recordings included interictal periods spanning up to 2 days before the first marked seizure. Seizure onset and termination were defined electrographically through visual inspection by two epileptologists (AD, MK) and led to a surgical intervention (laser interstitial thermal therapy) with a very good post-surgical outcome (Engel I) after a follow-up of 2 years and a half (Table I).

Additionally, we analyzed 10 patients from the publicly available SWEC-ETHZ iEEG long-term database (http://ieeg-swez.ethz.ch/) (Figure S1), produced through a joint initiative between the Sleep-Wake-Epilepsy-Center at the University Department of Neurology, Inselspital Bern, and the Integrated Systems Laboratory, ETH Zurich. This dataset consists of over 2,500 hours of continuous sEEG recordings across 18 patients. For this study, only patients with more than 2 days of recordings before their first seizure were considered. The selected patients, labeled as P2 to P11 for consistency, correspond to IDs 01, 02, 03, 11, 12, 14, 15, 16, 17, and 18 in ascending order from the original database. The number of electrodes varied across patients, ranging from 24 to 98 (Table I).

Table 1. Data of patients included in the study.

Patient	Gender /Age	Epilepsy onset (years)	Suspected epileptic focus	Hand laterality	Implantation	Number of electrodes (right/left)	Number of channels included in the analysis	Recorded time before first seizure onset (hours)	Magnetic Resonance	Surgery	Coregistered EKG	Outcome (2 y ½)
1	M/30	18	R lateral frontal	R	Bilateral	3/14	172	66	Normal	LITT	Yes	Engel I
2	N/A	N/A	N/A	N/A	N/A	N/A	88	121	N/A	N/A	No	N/A
3	N/A	N/A	N/A	N/A	N/A	N/A	66	230	N/A	N/A	No	N/A
4	N/A	N/A	N/A	N/A	N/A	N/A	64	84	N/A	N/A	No	N/A
5	N/A	N/A	N/A	N/A	N/A	N/A	32	183	N/A	N/A	No	N/A
6	N/A	N/A	N/A	N/A	N/A	N/A	56	82	N/A	N/A	No	N/A
7	N/A	N/A	N/A	N/A	N/A	N/A	24	88	N/A	N/A	No	N/A
8	N/A	N/A	N/A	N/A	N/A	N/A	98	42	N/A	N/A	No	N/A
9	N/A	N/A	N/A	N/A	N/A	N/A	34	111	N/A	N/A	No	N/A
10	N/A	N/A	N/A	N/A	N/A	N/A	60	84	N/A	N/A	No	N/A
11	N/A	N/A	N/A	N/A	N/A	N/A	42	93	N/A	N/A	No	N/A

EKG = electrocardiogram; R = right; LITT = laser interstitial thermal therapy

Data preprocessing

The recorded data were exported from Natus NeuroWorks software. For the primary patient, recordings consisted of 172 channels spanning 2 days prior to the first marked seizure, with sEEG and EKG signals acquired in a referential configuration at a sampling rate of 2048 Hz. Channels exhibiting artifacts were identified and excluded by one epileptologist (AD). The signals were re-referenced to a common external electrode, and to optimize computational efficiency, the data were down sampled to 512 Hz. Detrending was applied to reduce long-term trends and systematic patterns, enabling the analysis of short-term signal fluctuations. Depending on the specific analysis, a band-pass Butterworth filter (1–150 Hz, 53 dB stopband attenuation, maximal ripples in passband 2%) was applied. Additionally, a notch filter at 50 Hz and its harmonics was used to eliminate power line interference.

General procedure

The initial objective was to replicate the findings of our previous study (Tauste Campo et al., 2018) in a new cohort of patients. Specifically, we assessed the emergence of transient high-connectivity network states (HCS) during the hours preceding seizure onset. Centrality entropy was evaluated for all sEEG signals, and time-matched comparisons were made between the hours preceding the first monitored seizure and the same time window on the previous day. According to our earlier results, a consistent drop in entropy on the seizure day was expected, primarily due to an increase in HCS probability. Further, we aimed to better understand the mechanisms underlying HCS and their connection to seizure generation by comparing HCS probability with other physiological and network-based variables, including signal power, heart rate, mean connectivity, and mean node centrality.

Power analysis

To compute normalized mean power, a baseline segment was first defined as the initial 5 minutes of recording on the first day to obtain the baseline power mean and standard deviation ($P_{baseline}$). After preprocessing the data, we estimated the power by integrating the power spectral density in the frequency band of interest according to previous studies (Vila-Vidal et al., 2020). Finally, we normalized the power values with respect to the baseline power ($P_{baseline}$) considering all channels. Then, we calculated the Z-score values (Z) using the mean and standard deviation of the baseline power (See Fig. S2 for a scheme illustration).

Heart rate analysis

The heart rate is defined as the number of heart beats per minute. The duration of each beat (t_{beat}) is usually estimated from the time interval between consecutive R-peaks. Heart rate analysis is a crucial component in the assessment of physiological states and the detection of potential abnormalities (Li et al., 2023). Preprocessing an electrocardiogram (EKG) signal is crucial for accurate heart rate calculation, as it removes noise and artifacts that can obscure the detection of R-peaks, which are pivotal for determining heart rate. The process typically involves filtering to remove baseline wander and power line interference, using high-pass, notch, and band-pass filters (Clifford, 2006). First, we down-sampled the raw EKG data from 2048 to 512 Hz. We mitigated the Baseline wander, caused by respiration and patient movement, with high pass Butterworth filtering around 0.5 Hz (53 dB stopband attenuation, maximal ripples in passband 2%). Then, we applied a notch filter at 50 Hz to remove the power line interference. Afterward, we use a bandpass Butterworth filter (53 dB stopband attenuation, maximal ripples in passband 2%) from 0.5 to 40 Hz to refine the signal by eliminating irrelevant high-frequency noise. To enhance the QRS complex and facilitate robust R-peak detection, additional processing steps, including differentiation, squaring, and moving window integration, were applied, following the Pan and Tompkins method (Pan & Tompkins, 1985). The heart rate (HR) was estimated as $HR = \frac{60}{t_{beat}}$. where t_{beat} is the interval between consecutive R-peaks (See Fig. S2 for a scheme illustration).

Functional connectivity analysis

The estimation of functional connectivity using Pearson correlation is a widely adopted method due to its simplicity and effectiveness in capturing linear relationships between time series data. Pearson correlation measures the strength and direction of the linear relationship between two signals by calculating the correlation coefficient, which ranges from -1 to 1, indicating perfect negative to perfect positive linear correlation, respectively (Pereda et al., 2005). This approach has been extensively applied in neuroimaging to construct functional connectivity networks by correlating the activity between brain regions (Friston, 2011). Its simplicity enables easy implementation and interpretation, although it may miss nonlinear interactions (Wendling et al., 2009). Let x and y be 2 N-length time series representing 2 recorded signals and let $\bar{x}$ and $\bar{y}$ be their respective sample means. Pearson correlation is computed as follows:

$$r(x,y) = \frac{\sum_{i=1}^{N}(x(i)-\bar{x})(y(i)-\bar{y})}{\sqrt{\sum_{i=1}^{N}(x(i)-\bar{x})^2}\sqrt{\sum_{i=1}^{N}(y(i)-\bar{y})^2}}. \quad (1)$$

For each patient and each consecutive 0.6-second window, we computed the absolute value of the correlation coefficient across all pairs of electrode channels.

Network states analysis

We evaluated network states by computing eigenvector centrality for each connectivity matrix, following the methodology described in (Tauste Campo et al., 2018). For a given graph $G = (V, E)$, let $A = (a_v, t)$ be its weighted adjacency matrix. The relative centrality score x_v of vertex $v \epsilon V$ can be defined as:

$$x_v = \frac{1}{\lambda}\sum_{t\epsilon V} a_{v,t} x_t, \quad (2)$$

which can be rearranged in a matrix form as $\lambda x = Ax$. According to the Perron-Frobenius theorem, the largest eigenvalue yields a valid centrality measure, provided that all entries in x are non-negative (Newman, 2010). The centrality measure is determined by the eigenvector corresponding to the largest eigenvalue of the absolute-valued connectivity matrix. The centrality value for the i -th channel is the i -th component of this eigenvector, with i ranging from 1 to the number of recording sites in a patient. Eigenvector centrality is self-referential; nodes have high centrality if they connect to other high-centrality nodes (Rubinov & Sporns, 2010). This measures each node's relative importance within the network.

By computing eigenvector centrality for each 0.6-second connectivity matrix, we generated independent centrality time series for all recorded channels across the entire session. Each connectivity matrix represents a distinct brain state (Allen et al., 2014), and changes in the matrix result in a rotation of the eigenvector, updating the channels' relative importance within the evolving network configuration (Tauste Campo et al., 2018). To quantify the variability of centrality dynamics, we estimated the multivariate Gaussian entropy of the centrality time series within consecutive, non-overlapping 180-second windows (300 samples), as a second-moment approximation of network variability. The entropy is defined as:

$$H_c = \frac{K}{2}(1 + \ln(2\pi)) + \frac{1}{2}\ln(\det \Sigma). \quad (3)$$

Here K is the number of recording sites, and Σ is the covariance matrix of the centrality time

series within the estimation window. In line with our previous findings, a significant decrease in centrality entropy prior to seizure onset is attributed to the increased occurrence of high-connectivity states (HCS). To identify spontaneous network states over long interictal periods (greater than 1 day), we clustered the eigenvector centrality sequences using the k-means algorithm. While k-means is computationally efficient and simple, it requires predefining the number of clusters k, and the algorithm's convergence may depend on the initial placement of centroids (Bizopoulos et al., 2013). In this study, we fixed $k = 12$ clusters per patient to capture a sufficiently wide range of visually inspected connectivity states, based on prior analyses of result stability across different cluster sizes (Tauste Campo et al., 2018).

Low-dimensional network model

We proposed a simplified statistical network model to simulate the emergence of high-connectivity states (HCS) in the preictal period. This model constrains mean functional connectivity and mean centrality values across non-overlapping time windows during the 4 hours preceding seizure onset, both on the seizure day and the corresponding period of the previous day. The model works by generating continuous signals whose sequential correlation matrices (normalized covariance matrices) are adjusted to meet predefined ranges for mean connectivity and centrality. To achieve a specific mean connectivity, the correlation matrix coefficients are iteratively adjusted until the desired mean connectivity value falls within a specified range. Next, to control mean centrality, the positions of the matrix coefficients are redistributed while keeping the mean connectivity constant. By altering the node positions rather than their values, mean centrality can be modulated independently of mean connectivity.

The model divides the preictal period into two stages: (1) From 2 to 4 hours before seizure onset, mean connectivity and mean centrality remain within the same ranges for both days, 0.2±0.01 for mean connectivity and 0.4±0.009 for mean centrality. (2) In the final 2 hours (from 0 to 2 hours before the seizure), the mean connectivity remains fixed at 0.25±0.01 for both days, while mean centrality increases only on the seizure day to 0.55±0.01.

From the covariance matrices generated by this model, eigenvector centrality values were extracted, enabling the identification of network states for both days. Subsequently, we calculated the time-varying probability of HCS using the same method applied to the real sEEG data. To ensure robust outcomes, the model was run 40 times, and results were averaged across all simulations.

Statistical analysis

To evaluate significant and sustained differences in time-varying measures such as mean power, mean connectivity, and centrality entropy, we employed a nonparametric cluster-based statistical test (Maris & Oostenveld, 2007). This test quantifies time-matched changes between variables recorded on the seizure day and the previous day. Specifically, we partitioned the continuous time series into non-overlapping segments of 20 minutes, corresponding to 20 consecutive biomarker samples. For each segment pair, we performed a Wilcoxon test (1,000 random permutations to determine statistical significance. Adjacent segments meeting a significance threshold of $P < 0.05$ over a minimum duration of 3 segments (1 hour) were grouped into clusters, and the mean significance within each cluster was considered the primary test statistic. The null distribution was obtained by calculating the test statistic for all possible reorganizations of the data groups (exact test).

To investigate the relationship between HCS probability and centrality entropy reduction (Fig. 2), we applied linear regression analysis and calculated the coefficient of determination (R^2). Additionally, mean connectivity values across electrode pairs were Fisher-transformed to stabilize variance and normalize the correlation coefficients (R. A. Fisher, 1915).

3. RESULTS

Pre-seizure HCS probability alterations

To investigate the pre-seizure specific emergence of high-connectivity states (HCS) in the new cohort of patients, we adopted the methodology from (Tauste Campo et al., 2018) (Fig. 1(a)). First, raw sEEG signal was segmented into non-overlapping 600 ms temporal windows (Fig. 1(a), top panel), followed by preprocessing steps detailed in the Methods section. For each temporal window, we computed the connectivity matrix using Pearson's correlation (Fig. 1(a), top middle), retaining the absolute values to calculate the mean connectivity and node centrality (also termed *centrality*). The eigenvector centrality was extracted from the absolute-valued correlation matrix, reducing the matrix from order NxN (where N is the number of channels) to a vector of N components, each representing the relative importance of a node within the network (Fig. 1(a), bottom middle). The centrality entropy, a measure of network state variability, was then calculated as the multivariate Gaussian entropy of 300 consecutive eigenvector vectors (non-overlapping), yielding an entropy value every 3 minutes (Fig. 1(a), bottom). Figure 1(b) shows time-varying calculations of mean power, connectivity, centrality, and centrality entropy for an exemplary patient (P1) on the seizure day and the preceding day, focusing on the four hours leading up to seizure onset. In (Tauste Campo et al., 2018), centrality entropy was shown to decline prior to seizure onset, correlating with an increase in HCS occurrence during this period.

Figure 2(a) illustrates the centrality entropy for patient Patient 1 (P1) on the seizure day and the preceding day, where a significant decrease in centrality entropy emerged approximately 2.5 hours before seizure onset. To define HCS, we employed the k-means clustering algorithm on centrality eigenvectors, ranking states in descending order of mean connectivity estimated via the Fisher transform (R. A. Fisher, 1915). Twelve distinct states were identified, with State 1 corresponding to the highest mean connectivity (HCS) and the last state representing the lowest (Fig. 2(b)). Next, we determined which state best explained the observed entropy decline using a linear regression model. Here, the dependent variable was the centrality entropy difference across days while the independent variable was the probability difference of each state. Figure 2(c) shows the coefficient of determination (R^2), revealing that the HCS (State 1) was the primary driver of the entropy drop. We then analyzed the HCS probability during the pre-seizure entropy decline window (0.5–2.5 hours before seizure onset), observing a significant increase in HCS probability on the seizure day compared to the previous day

(randomization test, $P < 0.01$). Figure 2(e) summarizes the time-varying dynamics of HCS probability over the 8 hours preceding seizure onset, highlighting a substantial increase in HCS probability as seizure onset approached, compared to the day before.

To validate the above findings, we reproduced the analyses using the publicly available SWEC-ETHZ iEEG database (18 patients). From these, 10 patients (P2–P11) met the inclusion criterion of having at least two days of recordings prior to the first monitored seizure. In 7 patients (P2–P6, P8, P11), a pre-seizure decline in centrality entropy was observed (Fig. S1(a)), replicating the results seen in P1 (Fig. 2(a)). Averaged across patients, HCS (State 1) consistently explained the entropy drop during the seizure day (Fig. S1(b)). Finally, the time-varying HCS probability revealed a patient-specific increase aligned with the entropy decrease on the seizure day (except for P6), supporting our hypothesis (Fig. S1C).

Robustness across sEEG montages

To assess the robustness of our findings to different electrode referencing schemes, we evaluated three standard montages: monopolar (used as baseline), bipolar, and common average reference (CAR). While monopolar references emphasize global effects, bipolar referencing enhances localized activity detection, and CAR mitigates global noise (Ball et al., 2009, Tian et al., 2023, Lachaux et al., 2003).

Figure 3(a) compares the coefficient of determination values for the three montages in the 8 hours preceding seizure onset. Across all cases, the HCS (State 1) remained the state most strongly associated with centrality entropy changes. Additionally, the time-varying HCS probability analysis (Fig. 3(b)) confirmed a significant pre-seizure increase (~2 hours before onset) across all montages. Interestingly, the bipolar montage exhibited the highest R^2 values and the most pronounced HCS probability increase in P1, suggesting that bipolar referencing may enhance the observed pre-seizure HCS dynamics.

Relationship of HCS probability with other physiological and network measurements

We evaluated the correlation between HCS probability and other estimated variables with physiological interpretation (mean sEEG signal power at different frequency bands, Figure 4(a); heart rate, Fig. 4(b)) as well as connectivity-based variables (mean sEEG connectivity, Fig. 4(c); mean sEEG centrality, Fig. 4(d)). For each case, we first estimated the coefficient of determination (R^2) between the probability of HCS and the corresponding variable (mean power, heart rate, etc.) over the time samples accumulated during the 8 hours preceding the

seizure onset time on both days (Left panels of Fig. 4; red: seizure day, blue: day before seizure). To examine how the correlation evolved over the above-considered 8 hours, we estimated the time-varying Spearman correlation (r) across windowed estimations of both HCS probability and the corresponding variable (Right panels of Fig. 4; red: seizure day, blue: day before seizure). Specifically, correlation values were estimated for each hour using 3-minute window samples with a step of 15 minutes. In addition, we represented the positive and negative threshold of the obtained the correlation coefficients based on their statistical significance (Fig. 4(b), $|r| > r_{\mathrm{th}} = 0.37, P < 0.05$).

The analysis of mean sEEG power revealed that HCS probability exhibited the strongest association with the ultra-slow (0.08–0.4 Hz), delta (1–4 Hz), theta (4–8 Hz), and gamma (30–80 Hz) bands (Fig. 4(a) left). The gamma band was further analyzed using time-varying Spearman correlation, which showed significant discontinuous positive correlations with HCS probability hours before seizure onset. However, near the seizure onset, this relationship transitioned to a negative correlation (Fig. 4(a) right). In the case of heart rate, the overall association with HCS probability was moderate, with R^2 values below 0.4 (Fig. 4(b) left). In contrast, the time-varying analysis revealed two distinct periods of significant negative correlation between heart rate and HCS probability: a sustained period from 5 to 2 hours before seizure onset and a brief period immediately preceding seizure onset. These findings suggest that increases in HCS probability during these periods coincide with reductions in the patient's heart rate (Fig. 4(b) right).

Mean functional connectivity showed very low R^2 values and no significant time-varying correlation, indicating that the dynamics of HCS, as inferred over short timescales (600 ms), are largely independent of the grand-average sEEG connectivity (Fig. 4(c)). Finally, the analysis of mean centrality revealed relatively high R^2 values on both days, reflecting that HCS are likely to represent a class of eigenvectors with large mean centrality. Accordingly, this association remained largely unspecific to the seizure day (Fig. 4(d)).

In summary, the strongest and most genuine association with HCS probability was observed for heart rate, suggesting a possible link between network connectivity and autonomic function. This relationship should be further investigated in larger patient cohorts, as it may reveal novel non-invasive biomarkers for pre-seizure periods. In particular, understanding the mechanistic basis for this association, particularly the role of cerebral blood flow and its connection to

network synchronizations, could provide valuable insights into seizure dynamics.

Pre-seizure enhanced HCS probability are driven by changes in SOZ node centrality

In Patient 1, the pre-seizure occurrence of more frequent high-connectivity states (HCS) (see Fig. 5(a) for examples of HCS and non-HCS samples) starting two hours before seizure onset (Fig. 5(b), top) was not fully associated with a consistent increase in the time-varying mean connectivity (Fig. 5(b), middle). This observation aligns with our earlier findings (Tauste Campo et al., 2018) and the correlation analysis presented in Fig. 4(c). In contrast, the time-varying mean centrality showed a pronounced deviation relative to the corresponding period on the previous day (Fig. 5(b), bottom). This prompted us to examine how the dynamics of node centrality influenced the emergence of HCS in this patient. To address this question, we first analyzed the mean centrality distribution across different type of channels, distinguishing between channels within the seizure-onset zone (SOZ), as identified by two epileptologists (AD, MK), and the remaining channels. Notably, the mean centrality of SOZ channels displayed a substantial increase during the two hours preceding the seizure compared to the previous day, mirroring the pattern of the overall mean centrality. In contrast, the mean centrality of non-SOZ channels exhibited more subtle alterations with respect to the previous non-seizure day (Fig. 5(c), top).

Next, we investigated whether the between-day increase in SOZ mean centrality was specifically associated with the HCS. An analysis across the 12 original states revealed that the pre-seizure increase in SOZ centrality was exclusively tied to the HCS (Fig. 5(c), middle). To confirm that this specificity was reciprocal, we compared the centrality of SOZ channels to a random subsample of channels of equal size. The increase in SOZ centrality was statistically significant ($P < 0.01$) (Fig. 5(c), bottom). These results indicate that the emergence of HCS during the pre-seizure period is driven by a specific increase in the mean centrality of SOZ channels.

At first glance, it may seem counterintuitive that states with identical mean connectivity can exhibit different mean centrality values. This discrepancy can be explained by a network model in which rearrangements within the connectivity matrix alter the centrality of certain nodes while preserving the overall connectivity (See next Section). Importantly, our data analysis revealed that no significant changes in mean connectivity were observed across days for every state, and only the centrality of SOZ channels in HCS was increased during the pre-seizure

period (Fig. S3).

In conclusion, our findings emphasize the critical role of SOZ-specific channels in driving the dynamics of HCS probability. Assessing the topological dynamics of these channels offers deeper insights into network-level changes that precede seizure onset and highlights the SOZ as a key contributor to the emergence of pre-seizure HCS.

A low-dimensional statistical network model reproduces the emergence of pre-seizure HCS probability

To further interpret the findings from Patient 1, we proposed a low-dimensional statistical network model (N = 4) designed to simulate the key network dynamics illustrated in Fig. 5. This model generated sequences of covariance matrices within a controlled range of mean connectivity values ensuring time continuous signals within each day and similar connectivity distributions across both days (Fig. 6(b), top right). However, during the two hours preceding seizure onset, the centrality distribution was altered between the two days by strategically rearranging the positions of correlation coefficients within the covariance matrices (Fig. 6(a)). Specifically, to manipulate mean centrality while maintaining constant mean connectivity, the coefficients within the correlation matrix were reorganized. This reconfiguration allows two matrices with identical mean connectivity to be classified into distinct states: high-connectivity states (HCS) and non-HCS. This distinction arises because the classification of network states prioritizes the structure of centrality (via eigenvectors) before ranking based on mean connectivity values. Fig. 6(a) demonstrates this principle: reorganizing the correlation coefficients to emphasize a hub channel (e.g., Ch1) increases the mean centrality (as observed on the seizure day), while an even distribution of coefficients produces a lower mean centrality (as seen on the day prior to seizure onset).

To explore the effects of these centrality changes on HCS probability, we analyzed the centrality dynamics of individual channels (Fig. 6(b) top left). When no single channel displayed prominent centrality (e.g., two to four hours before the seizure), the HCS probability remained relatively stable (Fig. 6(b), bottom right). In contrast, when a specific channel (Ch1) dominated centrality, a significant increase in HCS probability was observed during the two hours leading up to the seizure (Fig. 6(b), bottom right). These results suggest that, within the model, channels exhibiting high centrality, analogous to the clinical seizure-onset zone (SOZ), play a key role in modulating both global mean centrality and HCS probability. This behavior

mirrors the real data, where the clinical SOZ channels predominantly shape the network's mean centrality dynamics and drive the emergence of HCS. The global mean connectivity and centrality remained stable over the simulated period (Fig. 6(b), top right and bottom left, respectively), reinforcing the interpretation that centrality changes—rather than connectivity variations—are responsible for pre-seizure increases in HCS probability.

The strength of this low-dimensional statistical network model lies in its ability to capture the observed pre-seizure behavior as an intrinsic network property. Specifically, the model demonstrates that an increase in HCS probability already arises when overall centrality becomes concentrated in a single channel as seizure onset approaches. This finding is further validated by averaging results across 40 independent simulations of the model, which replicates the pre-seizure emergence of HCS seen in the experimental data.

4. DISCUSSION

In this study, we explored the occurrence of high-connectivity states (HCS) as a potential biomarker for identifying pre-seizure periods using intracranial EEG (sEEG) recordings from patients with drug-resistant epilepsy. Building on previous research (Tauste Campo et al., 2018), we validated and expanded their findings in a new cohort of 11 patients, revealing a significant pre-seizure decrease in centrality entropy driven by increased HCS probability. Additionally, we examined the robustness of HCS probability under different sEEG referencing montages, analyzed its correlation with other physiological and connectivity-based variables, and developed a low-dimensional statistical network model to simulate the observed pre-seizure dynamics.

Multi-patient validation

We extended our earlier findings to a new cohort of 11 patients, consisting of Patient 1 from a collaborating hospital and Patients 2–11 from a publicly available online database. In 8 out of 11 patients, centrality entropy significantly decreased within up to 8 hours preceding seizure onset, a reduction that we attributed to an increase in HCS probability. However, the 10 patients from the online database provided limited metadata, including seizure onset times but lacking crucial clinical details such as electrode labels, co-registered electrocardiogram (ECG), and validated seizure-onset zones (SOZ). As a result, a more detailed analysis was performed only in Patient 1, where richer clinical and physiological data were available. For this patient, we explored the robustness of HCS probability across different referencing montages, investigated its correlation with heart rate and other physiological and connectivity variables, and assessed the influence of SOZ dynamics on HCS probability.

Considerations on robustness analysis and correlation with other predictive variables

The robustness of HCS probability was confirmed across monopolar, common average, and bipolar sEEG montages, where we consistently observed significant increases in HCS probability hours before seizure onset, with high coefficients of determination. To further interpret HCS probability within a broader physiological and functional connectivity framework, we compared it with other previously studied variables, including sEEG signal power (Vila-Vidal et al., 2017), heart rate (Karoly et al., 2021), mean connectivity, and mean centrality. While HCS probability increased almost uniformly across physiological frequency bands, gamma-band power correlations fluctuated near significance thresholds over time. In contrast, heart rate displayed sustained significant correlations between 2 to 5 hours and again

30 minutes before seizure onset. Mean connectivity consistently exhibited low correlations with HCS probability, while mean centrality showed relatively higher correlations. These results suggest that heart rate and mean centrality could complement HCS probability, providing a multidimensional perspective for predicting epileptic seizures (Schlegel et al., 2024).

Insights from a low-dimensional statistical network model

To explain the observed pre-seizure increases in HCS probability, we developed a low-dimensional statistical network model ($N = 4$ nodes) that captures key topological changes in brain connectivity. Network dynamic models are particularly valuable for analyzing the time-varying interactions that drive seizure generation (Sriraam et al., 2018). In our study, we observed that both mean connectivity and mean centrality increased two hours prior to seizure onset; however, only mean centrality showed a significant and sustained change with respect to the previous non-seizure day. This observation led to design a network model based on covariance matrices that preserved mean connectivity but allowed variations in centrality by rearranging the positions of correlation coefficients.

The model demonstrated that changes in mean centrality, rather than mean connectivity, might drive the emergence of HCS probability. Specifically, when centrality was evenly distributed across the network, HCS probability remained stable during the pre-seizure period (2–4 hours before seizure onset). However, when centrality became concentrated in a single hub node, HCS probability significantly increased closer to seizure onset (0–2 hours before the event). Averaging across a number of simulations, we found that enhanced HCS probability emerged as an intrinsic property of the network when centrality dynamics became dominated by a subset of nodes, resembling the behavior of SOZ channels observed in real data. Thus, the network model highlights the critical role of centrality dynamics in driving pre-seizure network behavior.

Study limitations

Despite the promising findings of this study, several limitations must be acknowledged. While heart rate and mean centrality emerged as potential complementary biomarkers to HCS probability, these observations were derived from a single patient with detailed clinical and physiological data. This limitation prevented us from integrating these variables into a unified predictive model. Future studies should address this by including a larger cohort of patients

with more complete metadata, such as epilepsy type, intracranial EEG montages, medication effects, and data from multiple seizures beyond the first monitored event. Another limitation lies in the use of Pearson correlation to measure functional connectivity, which is effective for capturing linear relationships but may fail to identify nonlinear signal dependencies. Exploring alternative connectivity measures that account for nonlinear interactions, such as phase-based or mutual information approaches, could reveal further insights into pre-seizure dynamics (Mercier et al., 2024).

The role of spontaneous interictal spikes, which are closely associated with seizure onset, also remains an important consideration for future research. Examining their distribution and behavior over extended pre-seizure periods may uncover additional predictive biomarkers for seizure onset (Karoly et al., 2016). Furthermore, heart rate variability (HRV) has been identified as a reliable pathological indicator of epilepsy (K. Li et al., 2023) , and its integration into predictive frameworks should be explored. Lastly, the use of our low-dimensional statistical network model provides an important avenue for simplifying network-level analyses. Future work should resort to such models to determine the minimum number of channels necessary for accurate seizure prediction. Reducing the dimensionality of seizure prediction models could improve clinical feasibility and computational efficiency, particularly in real-world applications (Statsenko et al., 2023).

5. CONCLUSION

In conclusion, our findings provide evidence that time-dependent increases in HCS probability throughout the day can serve as a potential pre-seizure biomarker. By combining detailed sEEG analysis with a low-dimensional network model, we propose that the preictal emergence of HCS reflects an intrinsic property of network organization primarily governed by centrality. Future research efforts aimed at integrating complementary physiological and connectivity-based measures into a unified, multivariate predictive framework could further enhance the clinical utility of HCS probability for reliable early detection of upcoming seizures.

ACKNOWLEDGEMENTS

N.M., M.V-V. and A.T.C were supported by the National Research project PID2020-119072RA-I00/AEI/10.13039/501100011033) funded by the Spanish Ministry of Science, Innovation, and Universities. N.M was supported by the predoctoral grant program "FI-SDUR" from the Department of Research and Universities, Catalan Government, 2022 (ref. BDNS 612831) (DOGC Núm. 8621 - 8.3.2022). M.V-V. was supported by the grant PTQ2022-012679, funded by the Spanish Ministry of Science, Innovation, and Universities.

AUTHOR STATEMENT

The authors declare no conflicts of interest.

ETHICAL STATEMENT

All diagnostic and surgical procedures were approved by The Clinical Ethical Committee of Hospital Clínic (HCB/2020/0182), and all clinical investigation was conducted according to the principles expressed in the Declaration of Helsinki. Following the Declaration of Helsinki, the patient was informed about the procedure, and they gave their written consent beforehand.

REFERENCES

Allen, E. A., Damaraju, E., Plis, S. M., Erhardt, E. B., Eichele, T., & Calhoun, V. D. (2014). Tracking Whole-Brain Connectivity Dynamics in the Resting State. Cerebral Cortex, 24(3), 663–676. https://doi.org/10.1093/cercor/bhs352

Billeci, L., Marino, D., Insana, L., Vatti, G., & Varanini, M. (2018). Patient-specific seizure prediction based on heart rate variability and recurrence quantification analysis. PLoS ONE, 13(9). https://doi.org/10.1371/journal.pone.0204339

Bizopoulos, P. A., Tsalikakis, D. G., Tzallas, A. T., Koutsouris, D. D., & Fotiadis, D. I. (2013). EEG epileptic seizure detection using k-means clustering and marginal spectrum based on ensemble empirical mode decomposition. 13th IEEE International Conference on BioInformatics and BioEngineering, 1–4. https://doi.org/10.1109/BIBE.2013.6701528

Clifford, g. d. (2006). a novel framework for signal representation and source separation: applications to filtering and segmentation of biosignals. Journal of Biological Systems, 14(02), 169–183. https://doi.org/10.1142/S0218339006001830

Cousyn, L., Dono, F., Navarro, V., & Chavez, M. (2023). Can heart rate variability identify a high-risk state of upcoming seizure? Epilepsy Research, 197, 107232. https://doi.org/https://doi.org/10.1016/j.eplepsyres.2023.107232

Fisher, R. A. (1915). Frequency Distribution of the Values of the Correlation Coefficient in Samples from an Indefinitely Large Population. Biometrika, 10(4), 507–521. https://doi.org/10.2307/2331838

Fisher, R. S., Scharfman, H. E., & de Curtis, M. (2014). How Can We Identify Ictal and Interictal Abnormal Activity? (pp. 3–23). https://doi.org/10.1007/978-94-017-8914-1_1

Friston, K. J. (2011). Functional and Effective Connectivity: A Review. Brain Connectivity, 1(1), 13–36. https://doi.org/10.1089/brain.2011.0008

Haneef, Z., Lenartowicz, A., Yeh, H. J., Levin, H. S., Engel, J., & Stern, J. M. (2014). Functional connectivity of hippocampal networks in temporal lobe epilepsy. Epilepsia, 55(1), 137–145. https://doi.org/10.1111/epi.12476

Karoly, P. J., Freestone, D. R., Boston, R., Grayden, D. B., Himes, D., Leyde, K., Seneviratne, U., Berkovic, S., O'Brien, T., & Cook, M. J. (2016). Interictal spikes and epileptic seizures: their relationship and underlying rhythmicity. Brain, 139(4), 1066–1078. https://doi.org/10.1093/brain/aww019

Karoly, P. J., Stirling, R. E., Freestone, D. R., Nurse, E. S., Maturana, M. I., Halliday, A. J., Neal, A., Gregg, N. M., Brinkmann, B. H., Richardson, M. P., La Gerche, A., Grayden, D. B., D'Souza, W., & Cook, M. J. (2021). Multiday cycles of heart rate are associated with seizure likelihood: An observational cohort study. EBioMedicine, 72. https://doi.org/10.1016/j.ebiom.2021.103619

Khambhati, A. N., Chang, E. F., Baud, M. O., & Rao, V. R. (2024). Hippocampal network activity forecasts epileptic seizures. Nature Medicine, 30(10), 2787–2790. https://doi.org/10.1038/s41591-024-03149-6

Lehnertz, K., Bröhl, T., & Wrede, R. von. (2023). Epileptic-network-based prediction and control of seizures in humans. Neurobiology of Disease, 181, 106098. https://doi.org/https://doi.org/10.1016/j.nbd.2023.106098

Li, K., Cardoso, C., Moctezuma-Ramirez, A., Elgalad, A., & Perin, E. (2023). Heart Rate Variability Measurement through a Smart Wearable Device: Another Breakthrough for Personal Health Monitoring? In International Journal of Environmental Research and Public Health (Vol. 20, Issue 24). Multidisciplinary Digital Publishing Institute (MDPI). https://doi.org/10.3390/ijerph20247146

Ludwig, K. A., Miriani, R. M., Langhals, N. B., Joseph, M. D., Anderson, D. J., & Kipke, D. R. (2009). Using a Common Average Reference to Improve Cortical Neuron Recordings From Microelectrode Arrays. Journal of Neurophysiology, 101(3), 1679–1689. https://doi.org/10.1152/jn.90989.2008

Maris, E., & Oostenveld, R. (2007). Nonparametric statistical testing of EEG- and MEG-data. Journal of Neuroscience Methods, 164, 177–190. https://doi.org/10.1016/j.jneumeth.2007.03.024

Mercier, M., Pepi, C., Carfi-Pavia, G., De Benedictis, A., Espagnet, M. C. R., Pirani, G., Vigevano, F., Marras, C. E., Specchio, N., & De Palma, L. (2024). The value of linear and non-linear quantitative EEG analysis in paediatric epilepsy surgery: a machine learning approach. Scientific Reports, 14(1), 10887. https://doi.org/10.1038/s41598-024-60622-5

Newman, M. (2010). Networks: An Introduction. Oxford University Press. https://doi.org/10.1093/acprof:oso/9780199206650.001.0001

Pan, J., & Tompkins, W. J. (1985). A Real-Time QRS Detection Algorithm. IEEE Transactions on Biomedical Engineering, BME-32(3), 230–236. https://doi.org/10.1109/TBME.1985.325532

Park, H. K., Jeong, J. H., Moon, S. Y., Park, Y. K., Hong, C. H., Na, H. R., Song, H.-S., Lee, S. M., Choi, M., Park, K. W., Kim, B. C., Cho, S. H., Chun, B.-O., & Choi, S. H. (2020). South Korean Study to Prevent Cognitive Impairment and Protect Brain Health Through Lifestyle Intervention in At-Risk Elderly People: Protocol of a Multicenter, Randomized Controlled Feasibility Trial. J Clin Neurol, 16(2), 292–303. https://doi.org/10.3988/jcn.2020.16.2.292

Pereda, E., Quiroga, R. Q., & Bhattacharya, J. (2005). Nonlinear multivariate analysis of neurophysiological signals. Progress in Neurobiology, 77(1), 1–37. https://doi.org/https://doi.org/10.1016/j.pneurobio.2005.10.003

Rubinov, M., & Sporns, O. (2010). Complex network measures of brain connectivity: Uses and interpretations. NeuroImage, 52(3), 1059–1069. https://doi.org/https://doi.org/10.1016/j.neuroimage.2009.10.003

Sander, D. (2013). Models of emotion: The affective neuroscience approach. In The Cambridge handbook of human affective neuroscience. (pp. 5–53). Cambridge University Press. https://doi.org/10.1017/CBO9780511843716.003

Sazgar, M., & Young, M. G. (2019). Overview of EEG, Electrode Placement, and Montages. In M. Sazgar & M. G. Young (Eds.), Absolute Epilepsy and EEG Rotation Review: Essentials for Trainees (pp. 117–125). Springer International Publishing. https://doi.org/10.1007/978-3-030-03511-2_5

Schlegel, K., Kleyko, D., Brinkmann, B. H., Nurse, E. S., Gayler, R. W., & Neubert, P. (2024). Lessons from a challenge on forecasting epileptic seizures from non-cerebral signals. Nature Machine Intelligence, 6(2), 243–244. https://doi.org/10.1038/s42256-024-00799-6

Sharma, A. K., Rani, E., Waheed, A., & Rajput, S. K. (2015). Pharmacoresistant Epilepsy: A Current Update on Non-Conventional Pharmacological and Non-Pharmacological Interventions. J Epilepsy Res, 5(1), 1–8. https://doi.org/10.14581/jer.15001

Sriraam, N., Raghu, S., Tamanna, K., Narayan, L., Khanum, M., Hegde, A. S., & Kumar, A. B. (2018). Automated epileptic seizures detection using multi-features and multilayer perceptron neural network. Brain Informatics, 5(2), 10. https://doi.org/10.1186/s40708-018-0088-8

Statsenko, Y., Babushkin, V., Talako, T., Kurbatova, T., Smetanina, D., Simiyu, G. L., Habuza, T., Ismail, F., Almansoori, T. M., Gorkom, K. N. V., Szólics, M., Hassan, A., & Ljubisavljevic, M. (2023). Automatic Detection and Classification of Epileptic Seizures from EEG Data: Finding Optimal Acquisition Settings and Testing Interpretable Machine Learning Approach. Biomedicines, 11(9). https://doi.org/10.3390/biomedicines11092370

Tauste Campo, A., Principe, A., Ley, M., Rocamora, R., & Deco, G. (2018). Degenerate time-dependent network dynamics anticipate seizures in human epileptic brain. PLoS Biology, 16(4). https://doi.org/10.1371/journal.pbio.2002580

Vandecasteele, K., De Cooman, T., Chatzichristos, C., Cleeren, E., Swinnen, L., Macea Ortiz, J., Van Huffel, S., Dümpelmann, M., Schulze-Bonhage, A., De Vos, M., Van Paesschen, W., & Hunyadi, B. (2021). The power of ECG in multimodal patient-specific seizure monitoring: Added value to an EEG-based detector using limited channels. Epilepsia, 62(10), 2333–2343. https://doi.org/10.1111/epi.16990

Vila-Vidal, M., Pérez Enríquez, C., Principe, A., Rocamora, R., Deco, G., & Tauste Campo, A. (2020). Low entropy map of brain oscillatory activity identifies spatially localized events: A new method for automated epilepsy focus prediction. NeuroImage, 208, 116410. https://doi.org/https://doi.org/10.1016/j.neuroimage.2019.116410

Vila-Vidal, M., Principe, A., Ley, M., Deco, G., Tauste Campo, A., & Rocamora, R. (2017). Detection of recurrent activation patterns across focal seizures: Application to seizure onset zone identification. Clinical Neurophysiology, 128(6), 977–985. https://doi.org/https://doi.org/10.1016/j.clinph.2017.03.040

Wendling, F., Bartolomei, F., & Senhadji, L. (2009). Spatial analysis of intracerebral electroencephalographic signals in the time and frequency domain: Identification of epileptogenic networks in partial epilepsy. In Philosophical Transactions of the Royal Society A: Mathematical, Physical and Engineering Sciences (Vol. 367, Issue 1887, pp. 297–316). Royal Society. https://doi.org/10.1098/rsta.2008.0220

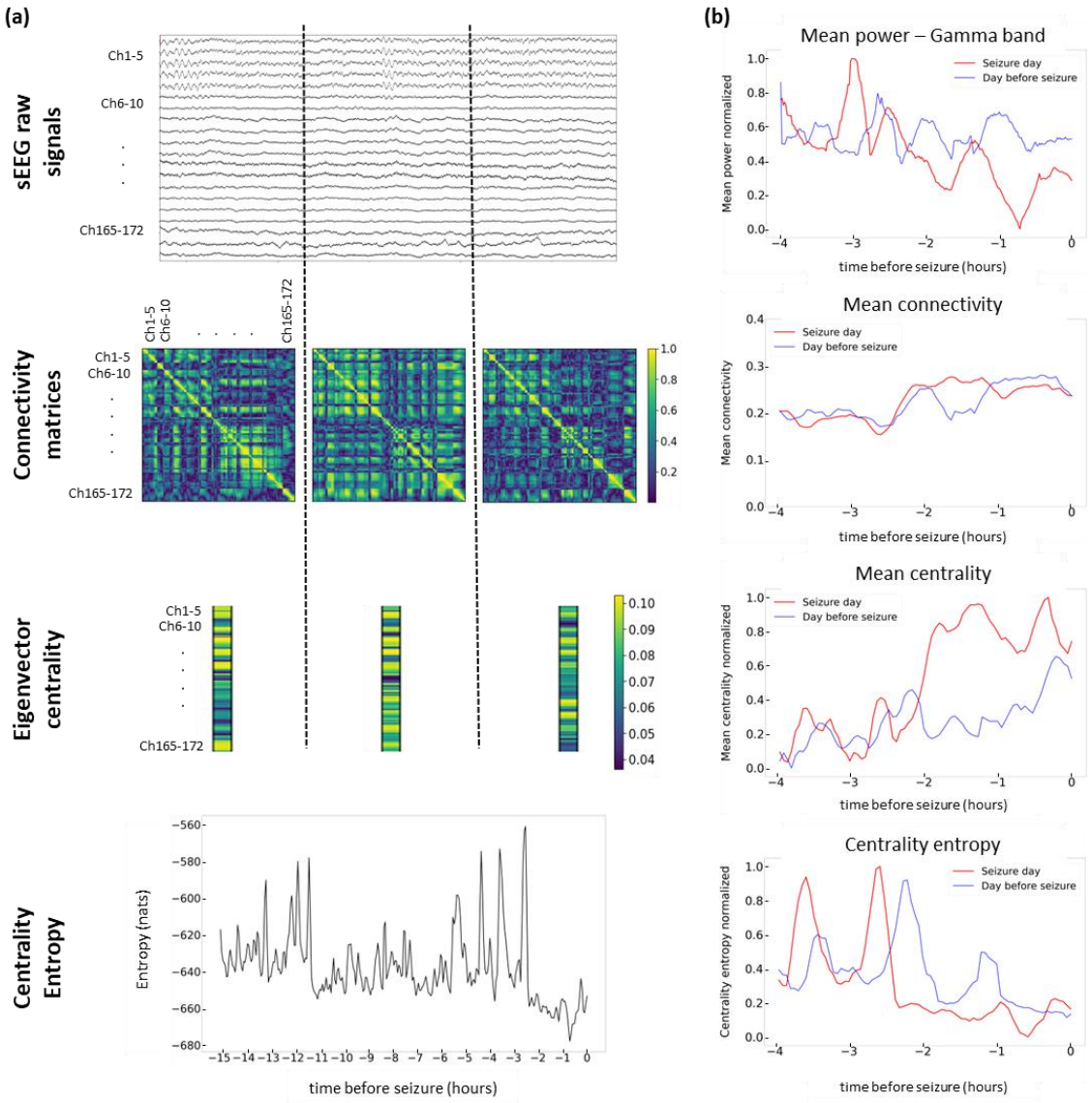

Fig. 1. Time-matched continuous sEEG network dynamics analysis across subsequent days. The procedure used in the previous study (Tauste Campo et al., 2018) to analyze the dynamics of the sEEG network during long continuous recordings is described step-by-step. 1(a) Top: Each sEEG signal is divided into consecutive and non-overlapping time windows of 0.6 seconds duration. The channels are grouped according to their corresponding electrodes. Top middle: Functional connectivity matrices are computed using the absolute value of the Pearson's correlation in each time window. Bottom middle: Eigenvector centrality is then calculated from each functional connectivity matrix to characterize transient network states. This approach transforms the NxN order matrix into an N-component vector that characterizes the network, where N is the number of channels. Bottom: The centrality entropy values are computed for each period of interest by sequentially estimating the multivariate Gaussian entropy of the eigenvectors in consecutive and non-overlapping time windows of 180 seconds (300 samples). 1(b) For an exemplary patient (P1) with 172 electrode channels, time-varying channel-averaged normalized outputs of each procedure step during the seizure day (in red) and the day before (in blue). Top: normalized mean power. Top middle, mean connectivity. Bottom middle: normalized mean centrality. Bottom: normalized centrality entropy. The centrality entropy values are also shown with the sampling rate of 1 sample every 3 minutes. The x-axis represents the time prior to the seizure, with the value 0 indicating the instant of seizure onset (reference). Ch, channel.

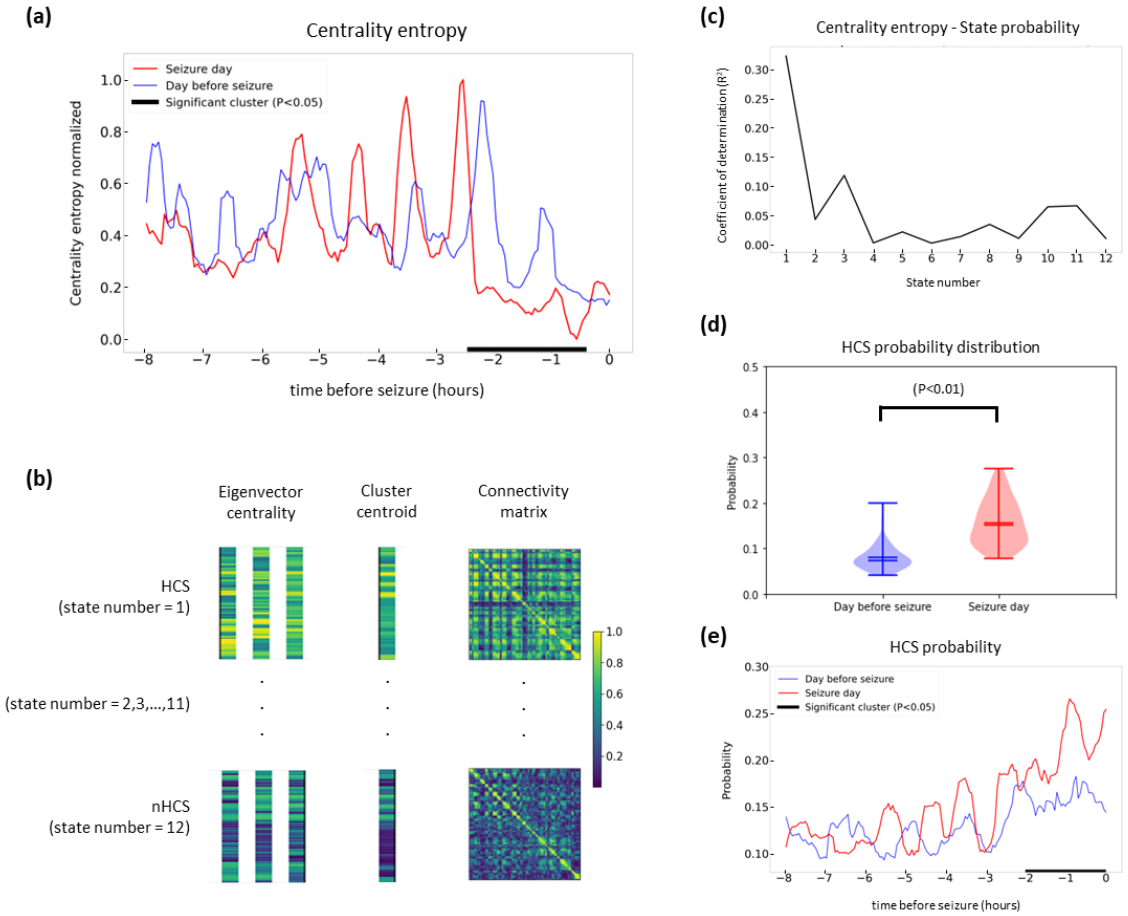

Fig. 2. Increased probability of high connectivity states (HCS) explains changes in pre-seizure sEEG network variability (Patient 1). 2(a) Centrality entropy was calculated for the day of the seizure (red) and the previous day (blue). The x-axis represents the time prior to the seizure in hours, with the value 0 marking the instant of seizure onset (reference). In this patient, a significant decrease in centrality entropy was observed from 2.5 to 0.5 hours before seizure onset ($P < 0.01$). 2(b) Definition of HCS and nHCS: Considering the entire data record, twelve states were defined and grouped in descending order according to their level of connectivity, with the first state corresponding to HCS and the last to the lowest connectivity. To cluster the centrality eigenvectors, an unsupervised K-means clustering algorithm was employed. Once the centrality centroids were defined for each 600 ms time window, they were ordered in decreasing order based on their mean connectivity. 2(c) The coefficient of determination (R^2) was calculated for a linear regression model where the dependent variable was the centrality entropy, and the independent variable was the state probability. The state that best explains the entropy drop is HCS (State 1), with an R^2 value above 0.3. 2(d) The distribution of HCS probability for both days during the critical period (from 0.5 to 2.5 hours before seizure onset) is shown. A significant increase in HCS probability ($P < 0.01$) is observed on the day of the seizure. 2(e) Finally, the dynamics of HCS probability over the 8 hours pre-ictal stage are depicted, illustrating a gradual increase in this parameter as the seizure onset approaches. The temporal window of significance occurs 2 hours before seizure onset ($P < 0.05$) which overlaps with the time window of the significant decrease of centrality entropy. In 1(a) and 1(e), the cluster-based permutation test was used to determine significance.

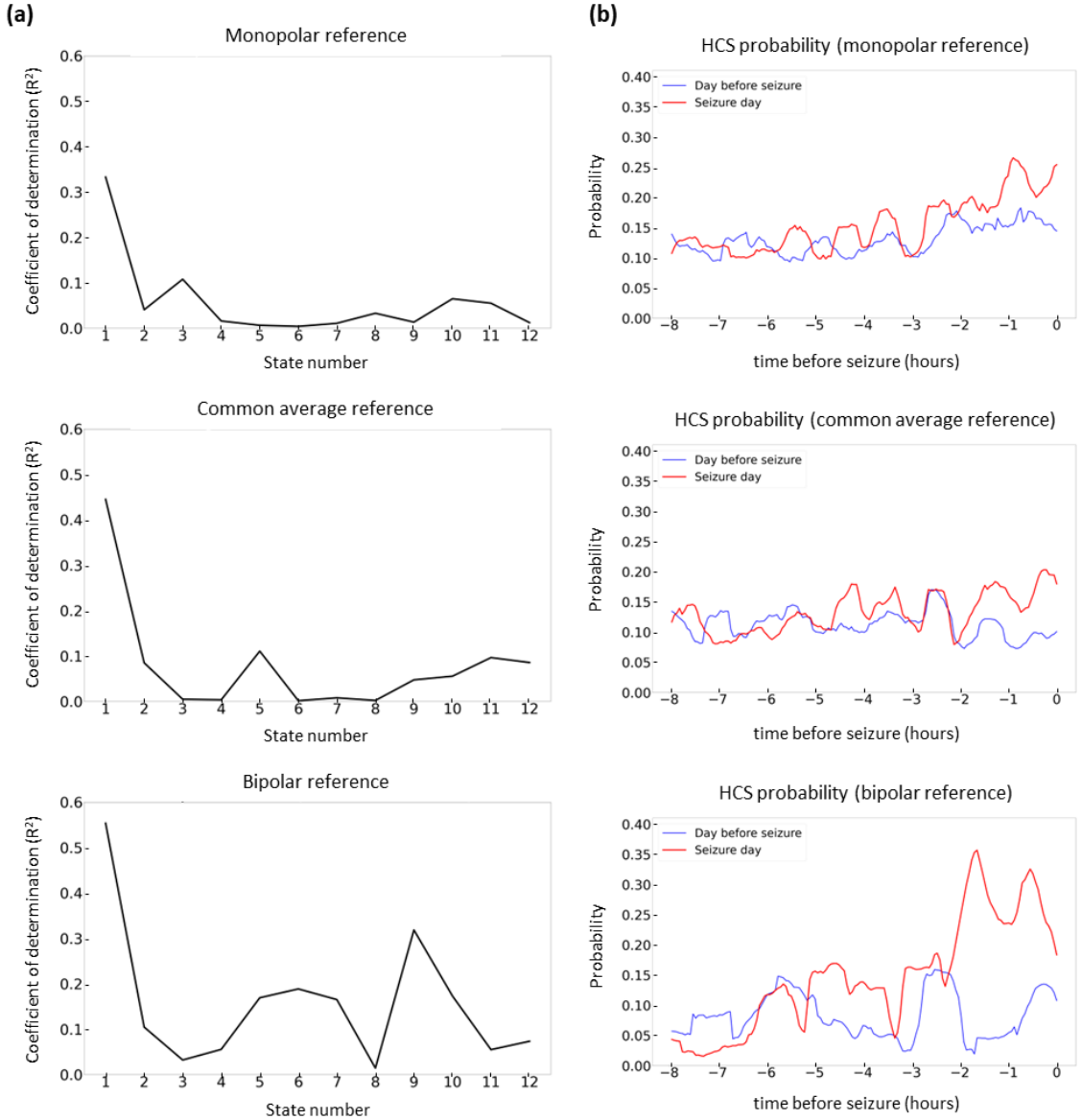

Fig. 3. Robustness of HCS pre-seizure emergence to reference montages (P1). Evaluation of HCS probability across three different reference montages: monopolar (top panels), common average (middle panels), and bipolar (bottom panels). The patient data were initially recorded with a monopolar reference. For the common average reference, the mean of all channels was subtracted from each individual channel, while for the bipolar reference, consecutive channels from the same electrode were subtracted. 3(a) The coefficients of determination (R^2) between centrality entropy and the probability of each state were calculated for each reference. In all montages, state 1 (HCS) best explained the entropy drop observed hours before seizure onset. The results remained consistent across reference configurations, with the highest R^2 value obtained in the bipolar montage (bottom panel). 3(b) The dynamics of HCS probability over the 8 hours prior to seizure onset for both the seizure day and the previous day are shown for each reference montage. In all cases, an increase in HCS probability as compared to the previous day was observed in the 2 hours leading up to seizure onset.

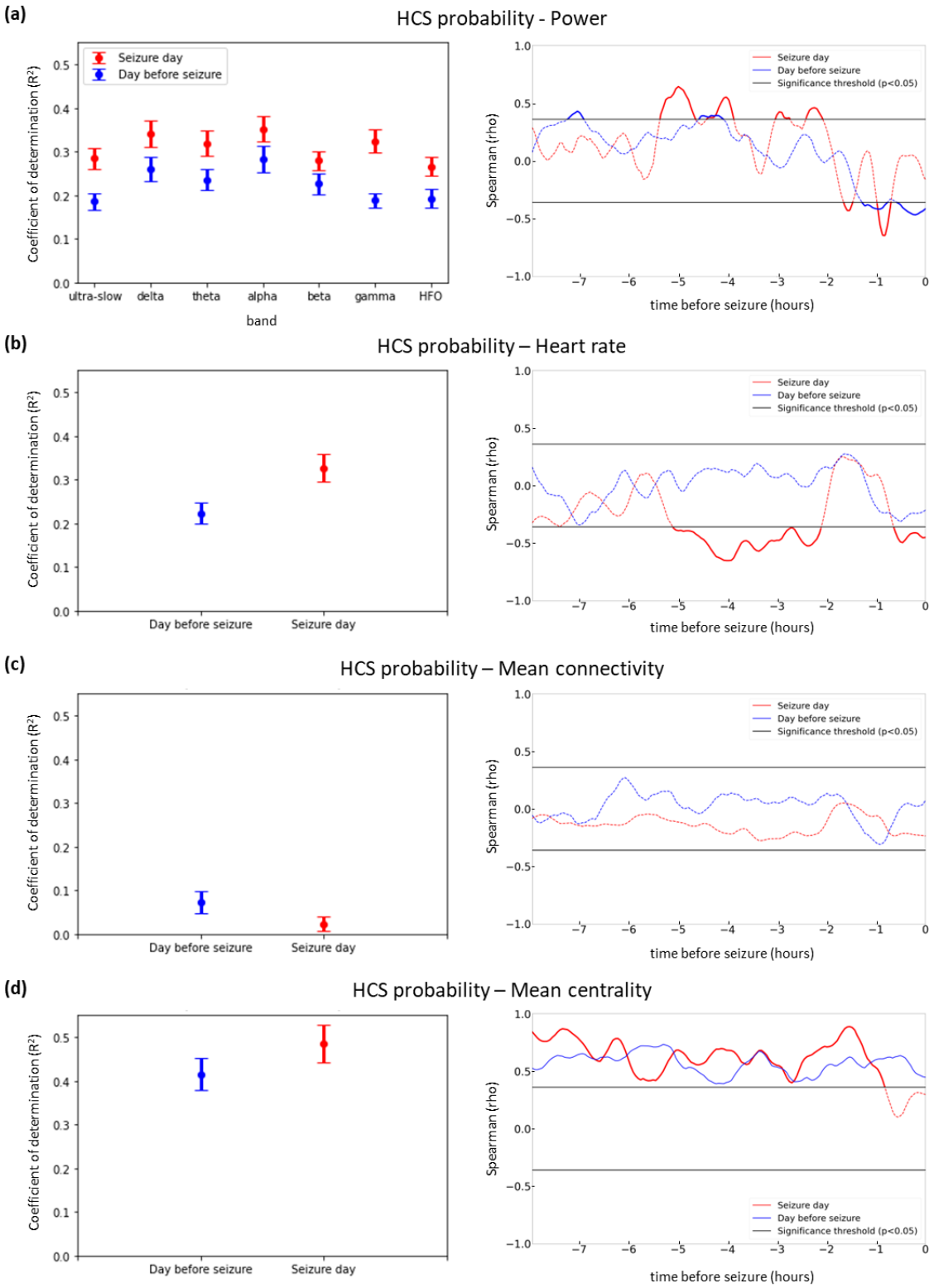

Fig. 4. Correlation between HCS probability and other stereo-encephalography (sEEG) and Electrocardiogram (ECK) variables (P1). The coefficient of determination (left panels) and the time-varying Spearman correlation (Spearman *rho*, right panels) between the probability of HCS and four different measurements on the seizure days (red) and on the day before seizure (blue) are computed. In the left panels, bootstrapping resampling was used to determine a confidence interval for the estimation of the coefficient of determination (R^2). In the right panels, black lines indicate the significance threshold ($P < 0.05$). 4(a) Left: Relationship between HCS probability and normalized power estimation at different physiological bands (ultra-slow,

0.08–0.4 Hz; delta, 1–4 Hz; theta, 4–8 Hz; alpha, 8-12Hz, beta, 12-30Hz; gamma 30–80 Hz; HFO, High-frequency oscillations, 80-150 Hz). Right: Time-varying correlation between the probability of HCS and normalized gamma power. 4(b) Left: Relationship between HCS probability and the heart rate. Right: Time-varying correlation between the probability of HCS and the heart rate. 4(c) Left: Relationship between HCS probability and the mean connectivity. Right: Time-varying correlation between the probability of HCS and the mean connectivity. 4(d) Left: Relationship between HCS probability and the mean centrality. Right: Time-varying correlation between the probability of HCS and the mean centrality.

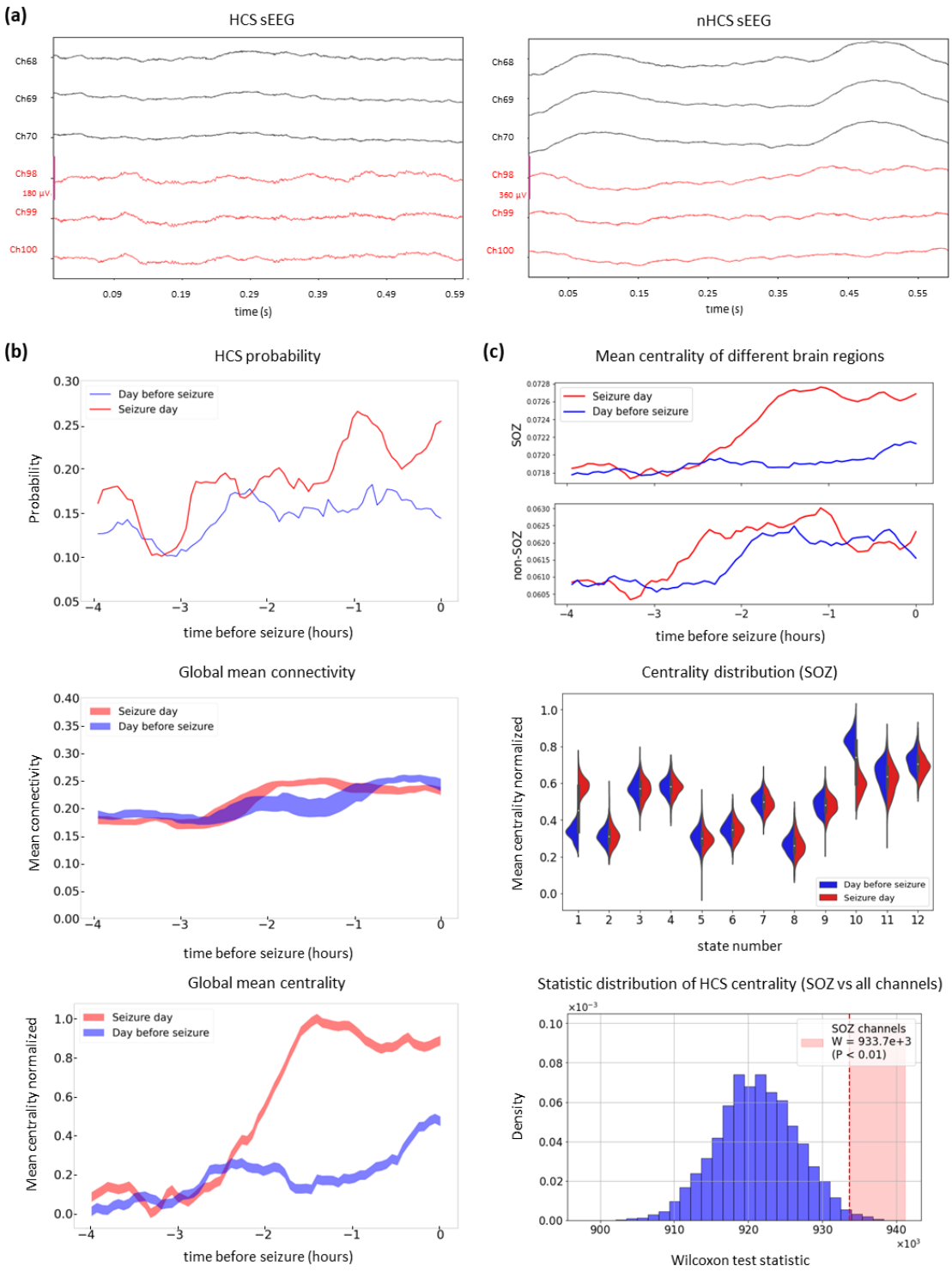

Fig. 5. Influence of the SOZ on pre-seizure HCS probability (P1). 5(a) Example 600 ms time windows of sEEG signals are shown for a high-connectivity state (HCS, left) and a non-high-connectivity state (nHCS, right). Signals from 3 seizure onset zone (SOZ) channels (red) and 3 non-SOZ channels (black) are included. In the HCS example, signal correlation is higher both within and outside the SOZ (global mean connectivity: 0.59; mean connectivity across six channels: 0.67), whereas in the nHCS example, correlations are lower (global mean connectivity: 0.18; mean connectivity across six channels: 0.24). 5(b) Time-varying connectivity-based metrics over the 4 hours preceding seizure onset on the seizure day (red) and the day before (blue). Top: HCS probability. Middle: Mean connectivity. Bottom: Mean centrality. 5(c) Top: Time-varying mean centrality

for SOZ channels (above, $n = 11$) and non-SOZ channels (below, $n = 161$) channels. Middle: Distribution of mean centrality for the SOZ across the 12 identified network states. Bottom: Surrogate distribution of the Wilcoxon test statistic built using 11 randomly selected non-SOZ channels, with the original test statistic highlighted by a red vertical dashed line ($P < 0.01$).

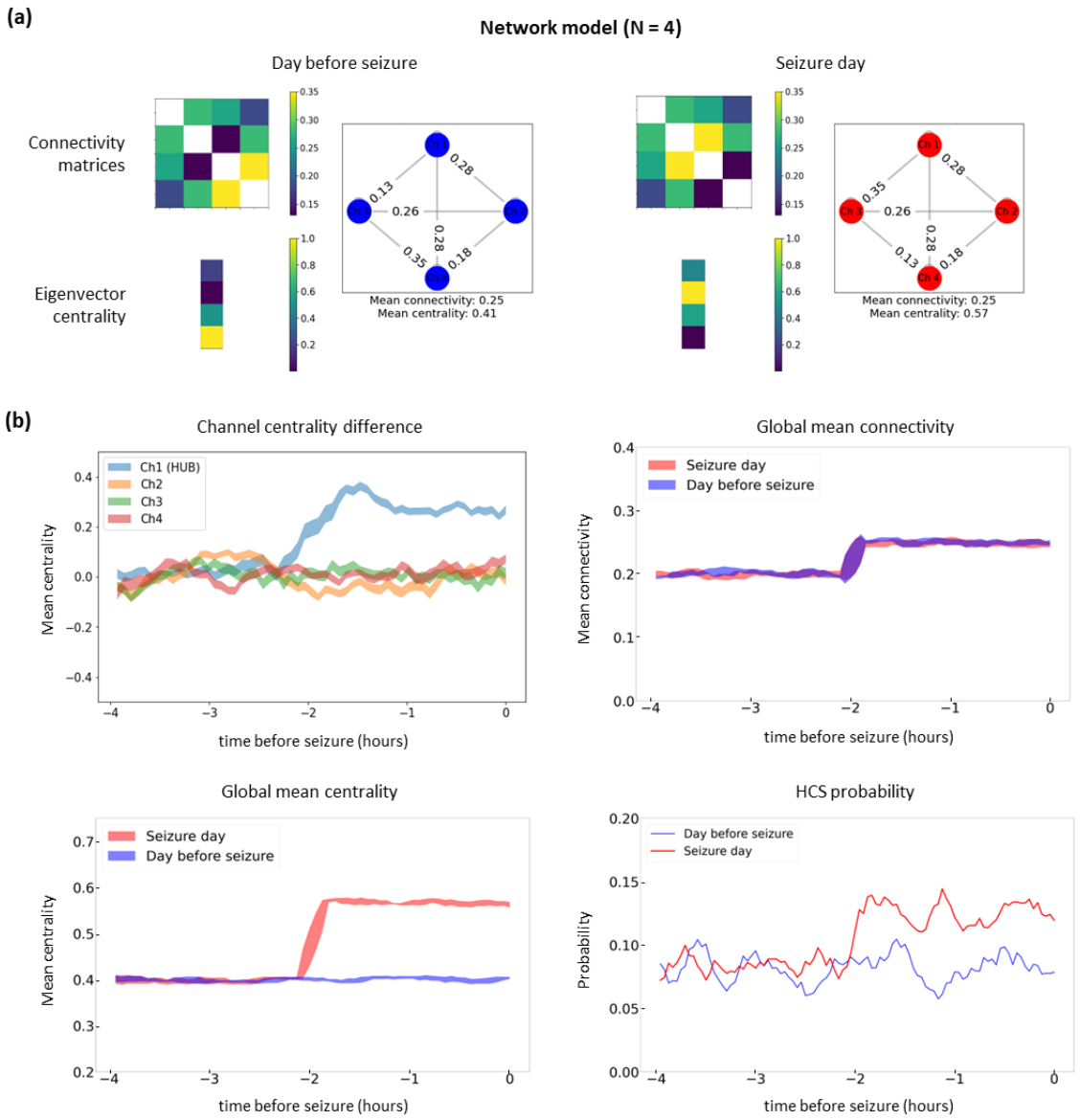

Fig. 6. Low-dimensional statistical network model. 6(a) The model generates random correlation matrices ($N = 4$) with fixed mean connectivity and varying mean centrality by rearranging correlation coefficients. This rearrangement produces two network states: one with uniform coefficient distribution (Left panel: lower centrality, as observed the day before the seizure) and another with a hub-like structure (Right panel: higher centrality, resembling the seizure day). Network states are classified based on eigenvector centrality, prioritizing centrality over connectivity. 6(b) Results averaged over 40 simulation runs. The four subfigures are interrelated, as they arise from the same set of simulations. The top left figure shows that HCS probability (bottom left) increases significantly only when a specific channel (e.g., Ch1) exhibits dominant centrality, forming a hub (analogous to the clinical SOZ). This centrality dominance explains the observed rise in HCS probability during the 2 hours preceding a seizure. The corresponding global mean connectivity and mean centrality are presented in the top right and bottom right figures, respectively. Together, these results demonstrate that the increase in HCS probability emerges as a topological property of the model.

Supplementary figures

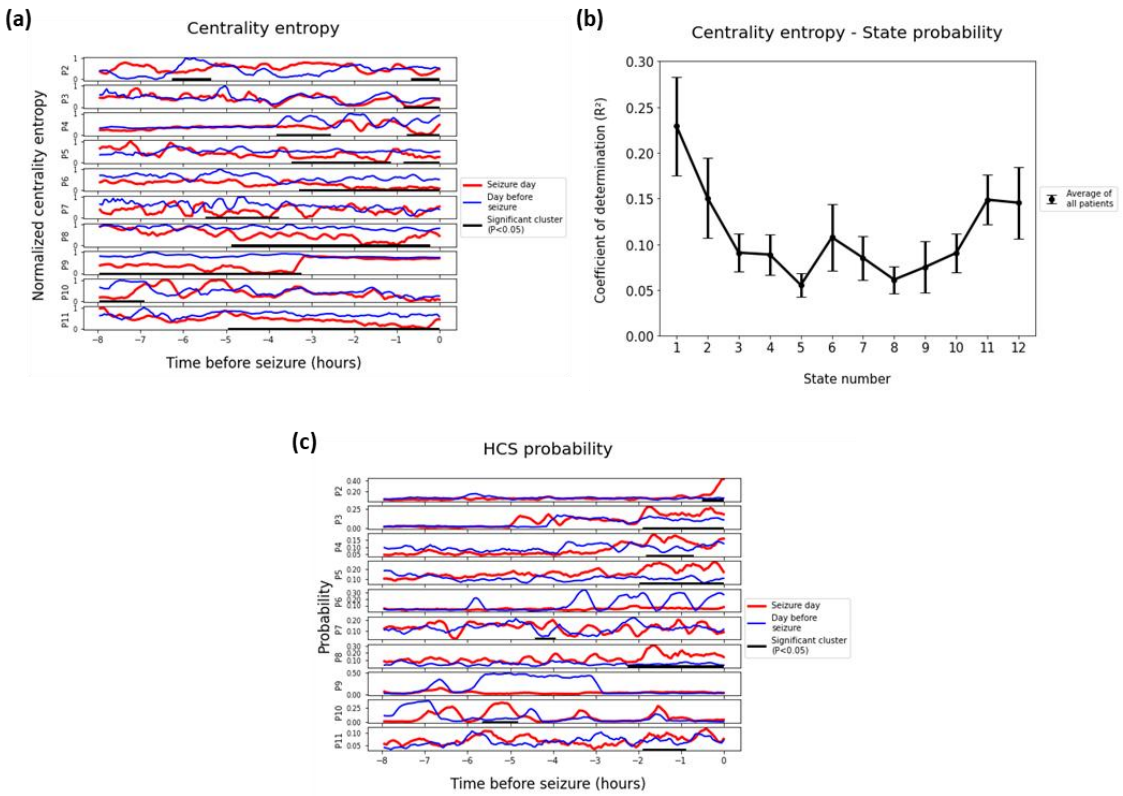

Fig. S1. Replication analysis in the SWEC-ETHZ iEEG Database. Ten patients (P2–P11) from the publicly available SWEC-ETHZ iEEG Database, meeting the criterion of having at least 48 hours of data recording before the first seizure, were analyzed. S1(a) The normalized centrality entropy was calculated for both days (red: seizure day; blue: day before the seizure). In 7 patients (P2, P3, P4, P5, P6, P8, and P11), a significant decrease in entropy was observed hours before seizure onset (Cluster-based permutation test, $P < 0.05$). S1(b) The patient-averaged coefficient of determination (R^2) was computed across the 12 clustered network states identified for each patient independently. S1(c) The probability of high-connectivity states (HCS) was calculated for both days. A significant pre-seizure increase in HCS probability was observed in 6 patients (P2, P3, P4, P5, P6, and P8).

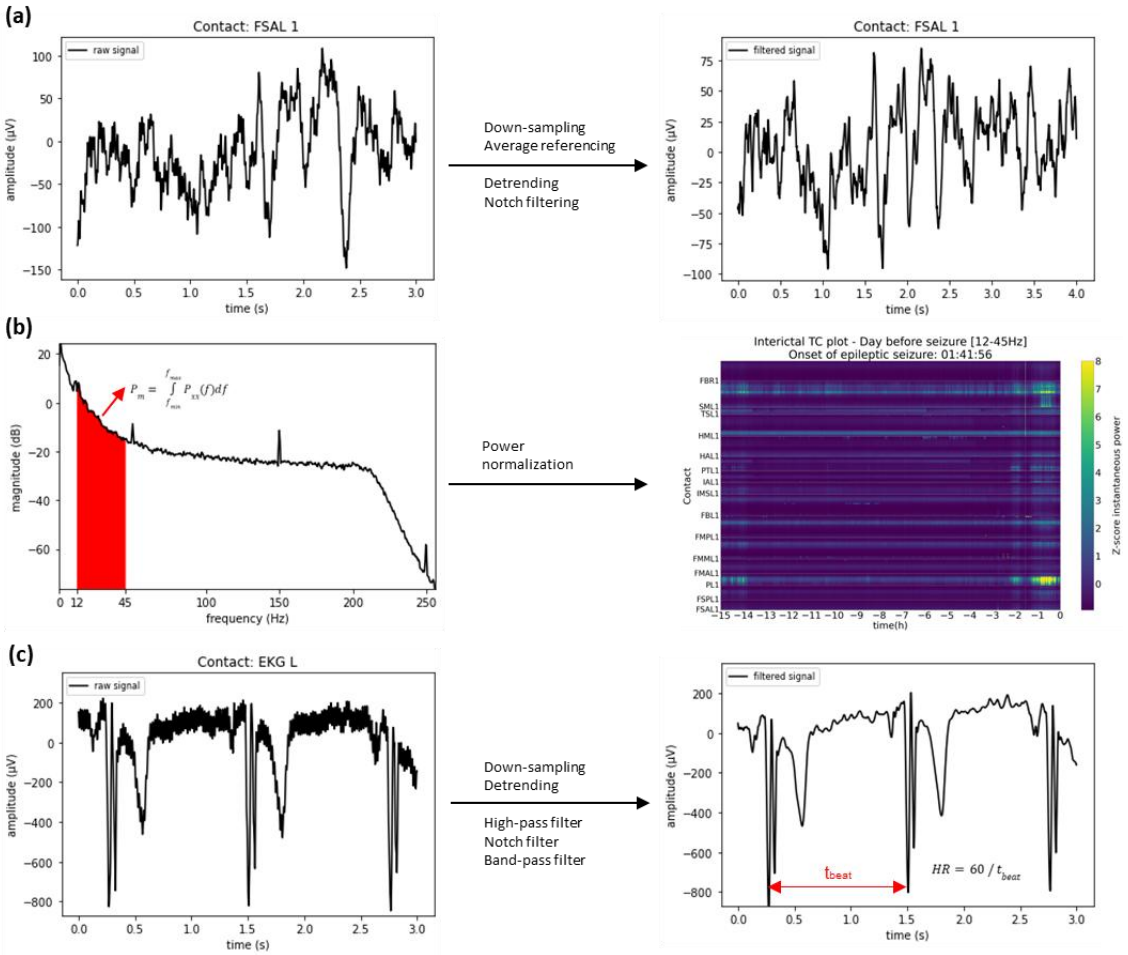

Fig. S2. Power and heart rate analysis. S2(a) sEEG signal preprocessing. Left: An exemplary raw sEEG signal is represented. Right: Preprocessing techniques (down-sampling, average referencing, detrending, and notch filtering) are applied to obtain a cleaner sEEG signal for analysis. S2(b) Power analysis. Left: The power spectral density (PSD) of the filtered signal is calculated and then integrated over the frequency range of interest (e.g. 12-45 Hz) to calculate power. Right: The power is normalized by computing its Z-score relative to a baseline defined as the first 5 minutes of the initial recording day. This spatio-temporal representation (time on the x-axis and channel contacts on the y-axis) illustrates an increase in power in specific channels (yellow) as the seizure approaches. S2(c) Heart rate analysis. Left: An exemplary raw EKG signal is represented. Right: Preprocessing steps (down-sampling, high-pass filtering [<0.5 Hz], notch filtering, band-pass filtering [0.5-40 Hz]) are applied to detect the time between R -peaks (t_{beat}) and calculate heart rate based on t_{beat}.

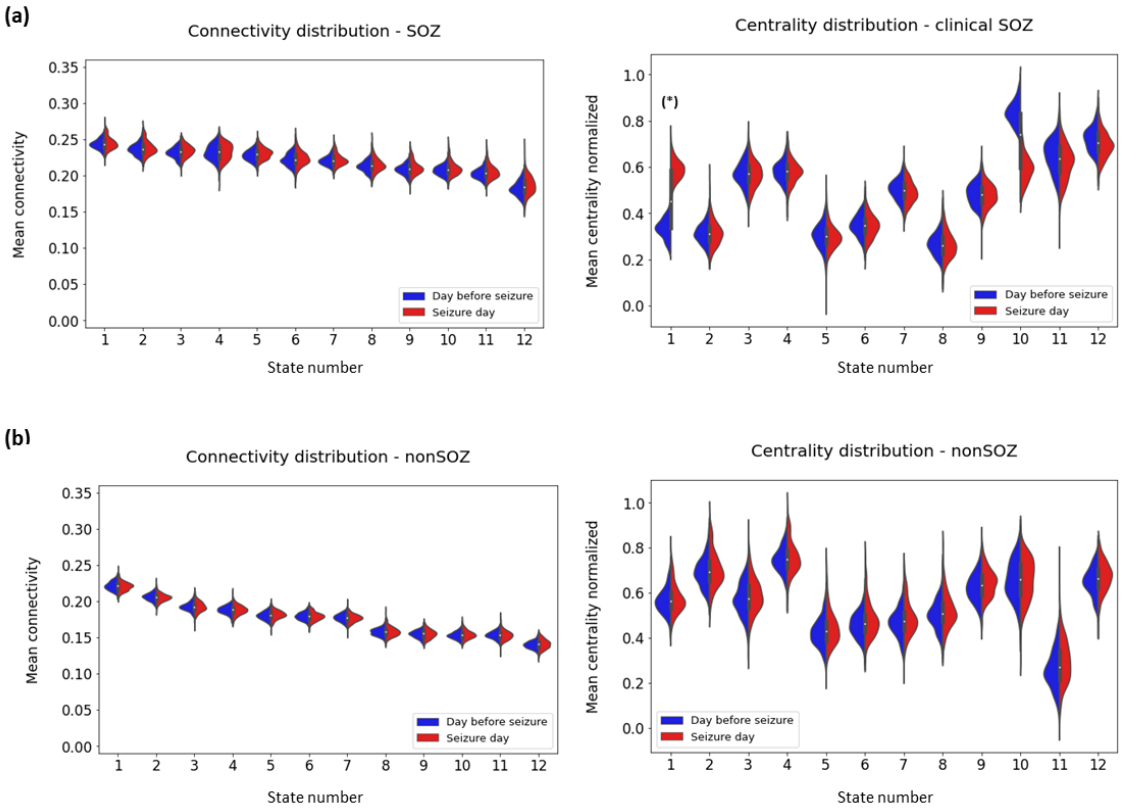

Fig. S3. Comparison of mean connectivity and mean centrality for SOZ and non-SOZ regions. The distributions of mean connectivity and mean centrality for the SOZ (A) and non-SOZ (B) channels during the 8 hours preceding the seizure are represented, with the seizure day shown in red and the previous day in blue. S3(a) SOZ channels. Left: The mean connectivity did not change significantly across both days for any network state. Right: A significant increase in centrality was observed in state 1, corresponding to the HCS (one-sided Wilcoxon testy, $P < 0.01$). Additionally, a difference of opposite sign arose in state 10 on the seizure day. S3(b) Non-SOZ channels. Left: No significant changes in mean connectivity were observed. Right: No significant changes in mean centrality were observed.